Ship resistance when operating in floating ice floes: a combined CFD&DEM approach

Luofeng Huang[a, *], Jukka Tuhkuri[b], Bojan Igrec[a], Minghao Li[c], Dimitris Stagonas[a, d], Alessandro Toffoli[e], Philip Cardiff[f], Giles Thomas[a]

[a]Department of Mechanical Engineering, University College London, United Kingdom
[b]Department of Mechanical Engineering, Aalto University, Finland
[c]Department of Mechanics and Maritime Science, Chalmers University of Technology, Sweden
[d]Department of Offshore Process and Energy Engineering, Cranfield University, United Kingdom
[e]Department of Infrastructure Engineering, University of Melbourne, Australia
[f] School of Mechanical and Materials Engineering, University College Dublin, Ireland

Abstract

Whilst climate change is transforming the Arctic into a navigable ocean where small ice floes are floating on the sea surface, the effect of such ice conditions on ship performance has yet to be understood. The present work combines a set of numerical methods to simulate the ship-wave-ice interaction in such ice conditions. Particularly, Computational Fluid Dynamics is applied to provide fluid solutions for the floes and it is incorporated with the Discrete Element Method to govern ice motions and account for ship-ice/ice-ice collisions, by which, the proposed approach innovatively includes ship-generated waves in the interaction. In addition, this work introduces two algorithms that can implement computational models with natural ice-floe fields, which takes randomness into consideration thus achieving high-fidelity modelling of the problem. Following validation against experiments, the model is shown accurate in predicting the ice-floe resistance of a ship, and then a series of simulations are performed to investigate how the resistance is influenced by ship speed, ice concentration, ice thickness and floe diameter. This paper presents a useful approach that can provide power estimates for Arctic shipping and has the potential to facilitate other polar engineering purposes.

Keywords: Ice Floe; Ship Resistance; Computational Fluid Dynamics; Discrete Element Method.

*Corresponding author: ucemlhu@ucl.ac.uk

1. Introduction

Global warming has induced a paradigm change in the Arctic environment, pronounced by an obvious transition from level-ice coverages to broken ice-floe fields and open water [1]. The changed condition makes the region more accessible to ships, with numerous waterways opening for travelling between continents and the Arctic, which are used to access oil, gas, mines, fishing grounds and tourism. Moreover, there are two major cargo-shipping routes becoming navigable, the Northwest Passage and the Northern Sea Route, which can be used as alternatives to the Panama and Suez canals to connect Europe, Asia and America; compared with their current counterparts, both new routes can reduce the travel distance by up to 40%, leading to significant fuel, cost, time and emission savings [2]. Under this trend, Arctic shipping is now attracting significant investment from commercial stakeholders and of special research interest.

Formidable challenges are coming hand-in-hand with the benefits of Arctic shipping. One of the most obvious is to understand the effect of the potential navigation environment on ships: instead of providing pure open water, level ice coverages are broken up into numerous ice floes floating on the sea surface. These ice floes, also known as pancake ice, tend to be circular under the effect of wave wash and floe–floe collisions, as shown in Figure 1. Such ice-floe fields have been predicted to be the most ubiquitous condition for future Arctic shipping [1], and it is also dominant in the Antarctic [3]. This has motivated experiments on ship advancement in ice floes [4–7], which reported the floes can induce significant resistance increments on the ship, indicating it is of great importance to predict the ice-added resistance. Nevertheless, considering the prohibitive costs of experiments and the shortage of field-measurement data, developing a reliable computational model to predict the ship performance with ice floes can be a cost-effective way to provide convenient solutions.

Successful modelling of broken ice-floe fields has been achieved using the Discrete Element Method (DEM), since this method allows the calculation of the contact force of ice-ice and ice-structure, which is essential for engineering problems in such ice-floe fields. A review on this has been given by Tuhkuri and Polojarvi [8]. Using DEM, Løset [9,10] calculated the force of an array of ice floes on a beam and found the load increases with an increased ice concentration, ice drift speed and the width of the beam, in which, the load appears to vary linearly with drift speed and beam width, while exponentially with ice concentration. Hopkins and Tuhkuri [11] simulated the jam of pancake ice floes in a trench and provided parallel experimental comparisons to show the overturning and rafting of floes can be decently modelled by DEM. Hopkins and Shen [12] further applied the method to replicate pancake-ice rafting in waves and the model was subsequently validated by the wave-tank experiments of Dai et al. [13]. Herman et al. [14–16] conducted combined numerical-experimental studies on wave attenuation through ice-floe fields, with DEM to account for the energy dissipation due to floe collisions.

Currently, one gap in related Discrete/Finite Element simulations is how to accurately account for the force of the surrounding fluid on the ice, which is usually implemented by empirical equations [8]. Due to this deficiency, previous simulations of a ship advancing in ice floes ignored the effect of fluid flow [7, 17–21], which reduces the reality of the modelling. The process of a ship advancing in floating ice floes can be summarised as the following ship-wave-ice interaction: ship advancement generates waves; waves interact with ice floes; ice floes contact each other and with the ship. The ship-generated waves can play a key role within the process; for example, it can change the velocity (magnitude and direction) of floes, especially when the floes are small. Therefore, ignoring the wave effect may considerably influence the ice load on a ship.

Tsarau et al. [22, 23] incorporated the potential-flow theory with DEM to better account for the fluid force on ice; however, recent experiments [24–26] have demonstrated that the linear assumptions applied in the potential-flow theory can cause inaccuracies in certain scenarios. For example, the theory excludes a phenomenon, overwash, defined as waves running over the top surface of floating ice [27], which can evidently suppress the movement of floes [25]. Since sea ice has very small freeboard due to its similar density with water, overwash is highly frequent in ship-wave-ice interactions. Thus, the exclusion of overwash makes the potential-flow theory less applicable to the proposed problem.

An alternative approach is to couple Computational Fluid Dynamics (CFD) with DEM, which allows for fully non-linear fluid solutions and is a very mature approach to model hydrodynamic problems [28]. CFD has been shown capable of simulating the motion of an ice floe in waves and has achieved good agreement with experiments when overwash occurs [29–31]. In addition, CFD is convenient for including complex geometries to study structure-wave-ice interactions, and it has been widely used to predict the resistance and wave making of an advancing ship [32, 33]. Other approaches have been found where the Lattice Boltzmann method (LBM) [34] or Smooth Particle Hydrodynamics (SPH) [34, 35] have been coupled with DEM to model the ship-wave-ice interaction; but the application and validation of SPH and LBM in ocean engineering are still rare when compared with CFD. One disadvantage of CFD comparing with theoretical predictions is that it needs much higher computational power. However, as DEM requests very high computational power itself, compared with using DEM solitarily, using CFD to provide fluid solutions for DEM will not significantly increase the required computational cost. Based on the above reasons, this study proposes to combine CFD with DEM to achieve the ship-wave-ice coupling.

Apart from accurately accounting for the fluid force, another challenge in the modelling of ice-floe fields is to import natural ice distributions into computational models. In polar regions, ice floes are randomly distributed and of a range of sizes [3,37]. Even though computational models are capable of simulating the structure-wave-ice interaction, the initial size and location of each floe need to be prescribed. For example, in the computational models of Janssen et al. [34], Sun and Shen [38] and

Huang et al. [39], ice floes are set to be of a uniform size and the distance between all ice floes is initialised to be the same, as shown in Figure 2; this is not a natural condition and the result can be subjected to initial setups (e.g. the relative positions between ship and floes considerably influence the ice resistance [39]). Therefore, there is the requirement to import natural ice distributions to realistically simulate the physical processes associated with floe fields.

The present paper presents a set of methods for modelling natural ice-floe fields and the simulation of a ship advancing in such an ice condition; subsequently, it focusses on investigating the ice-added resistance on the ship. Section 2.1 and 2.2 demonstrate the CFD and DEM methods applied in the proposed problem and how they are coupled together to model the ship-wave-ice interaction; Section 2.3 presents the development of two algorithms that can generate ice-floe distributions according to practical observations, which is used to initialise ice conditions for the CFD&DEM model. Following the completeness of the model, Section 3 provides the prediction and validation of ship resistance in ice floes and shows how the resistance is influenced by ship speed, ice concentration, ice thickness and floe diameter. The CFD&DEM approach is demonstrated to simulate the new shipping scenario with high fidelity and could be used to provide valuable insights for other Arctic engineering purposes.

Figure 1: A ship advancing in floating ice floes (photo credit: Alessandro Toffoli).

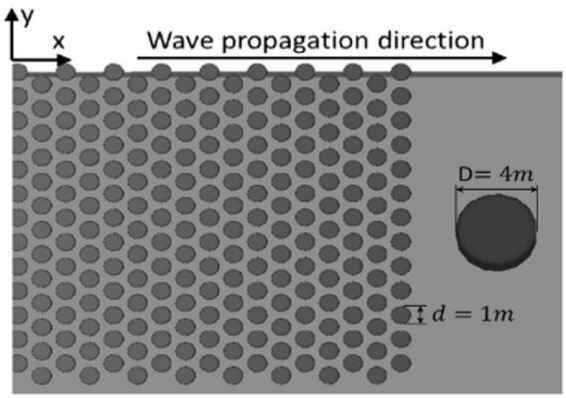

Figure 2: Regular pancake-ice field used by Sun and Shen [38].

2. Computational modelling

In order to simulate a ship advancing in floating ice floes, this work followed three steps to build a computational model: (a) CFD, a standard model of ship advancement in open water, where fluid solutions are obtained, including the wake and water resistance of a ship. (b) DEM, for modelling ice floes and their collisions with the ship and nearby floes; those floes obtain fluid force from the CFD solution so that the ship-wave-ice coupling is achieved. (c) floe-distribution algorithms, by which natural ice-floe fields are generated and implemented into the CFD&DEM model. Steps (a) and (b) were performed based upon the STAR-CCM+ software, and Step (c) was realised using MATLAB scripts.

2.1 CFD ship flow

A modern container ship model, KRISO Container Ship (KCS), was adopted as the ship model for this study. KCS is a typical container ship model employed in computational simulations, and its geometry with appendages is openly accessible [40]. The length of the hull is 230 m at full-scale with a scale ratio of 1:52.667 applied in this study for the purpose of validation, resulting in a model length L_{pp} = 4.367 m and breadth B = 0.611 m. The hull parameters are summarised in Table 1.

Table 1. Main dimensions of the KCS hull.

	Model scale	Full scale
Length between perpendiculars (m)	4.367	230.0
Waterline breadth (m)	0.611	32.2
Draught midships (m)	0.205	10.8
Trim angle (rad)	0.0	0.0
Block coefficient (-)	0.651	0.651
Wetted surface area (m^2)	3.397	9424.0

Following the guidelines of the International Towing Tank Conference [41], an open-ocean fluid domain was built with the recommended domain size and boundary conditions, as shown in Figure 3. The computational domain is three-dimensional, defined by the earth-fixed Cartesian coordinate system

O-*xyz*. The (*x*, *y*) plane is parallel to the horizon, and the *z*-axis is positive upwards. The domain size is sufficiently large to avoid the ship-generated waves being reflected from the boundaries. The lower part of the domain is filled with water and the remainder is filled with air. The hull is fixed at the free surface according to its design draught and the hull surface is modelled as a no-slip wall. The water was initialised as flowing with a constant velocity (U_{water}) against the bow of the hull, and a constant velocity condition was applied to the inlet boundary to maintain a stable water flow entering the domain. Thus, a relative velocity exists between the ship and water, where U_{water} indicates the advancing speed of the ship in calm water. The ship speed can be converted to Froude number $Fr = U/\sqrt{g \times L_{pp}}$, where g and L_{pp} are gravitational acceleration and ship length respectively. The fixed-dynamic-pressure condition is applied to the outlet, and the zero-gradient condition is applied to other boundaries.

The solution of the fluid domain was obtained by solving the Reynolds-averaged Navier-Stokes (RANS) equations for an incompressible Newtonian fluid:

$$\nabla \cdot \overline{\mathbf{v}} = 0 \tag{1}$$

$$\frac{\partial(\rho\overline{\mathbf{v}})}{\partial t} + \nabla \cdot (\rho\overline{\mathbf{v}}\overline{\mathbf{v}}) = -\nabla\overline{p} + \nabla \cdot \left(\overline{\tau} - \rho\overline{\mathbf{v}'\mathbf{v}'}\right) + \rho g \tag{2}$$

where $\overline{\mathbf{v}}$ is the time-averaged velocity, $\mathbf{v}'$ is the velocity fluctuation, ρ is the fluid density, $\overline{p}$ denotes the time-averaged pressure, $\overline{\tau} = \mu[\nabla v + (\nabla v)^T]$ is the viscous stress term, μ is the dynamic viscosity and g is gravitational acceleration set at 9.81 m/s^2. Since the RANS equations have considered the turbulent fluid, the Shear Stress Transport (SST) k − ω model [42] was adopted to close the equations. The SST k − ω model has been proposed to be the most appropriate option among standard RANS turbulence models for predicting the flow field around a ship hull [43].

The free surface between the air and water was modelled by the Volume of Fluid (VOF) method [44]. The VOF method introduces a passive scalar α, denoting the fractional volume of a cell occupied by a specific phase. In this case, a value of α = 1 corresponds to a cell full of water and a value of α = 0 indicates a cell full of air. Thus, the free surface, which is a mix of these two phases, is formed by the cells with $0 < \alpha < 1$. The elevation of the free surface along time is obtained by the advection equation of α, expressed as Equation (3). For a cell containing both air and water, its density and viscosity are determined by a linear average according to Equation (4) and Equation (5). In this study, ρ_{water} = 998.8 kg/m^3, $\mu_{water} = 8.90\times10^{-4}$ N·s/m^2; ρ_{air} = 1 kg/m^3, $\mu_{air} = 1.48\times10^{-5}$ N·s/m^2. The governing equations of the fluid domain were discretised and solved using the Finite Volume method [45]; Figure 4 shows the mesh layout of the model, in which high resolutions are applied to the regions where ship-wave-ice interactions are expected to happen, resulting in a total cell number of around three million.

$$\frac{\partial \alpha}{\partial t} + \nabla \cdot (\overline{\mathbf{v}}\alpha) = 0 \tag{3}$$

$$\rho = \alpha\rho_{water} + (1-\alpha)\rho_{air} \tag{4}$$

$$\mu = \alpha\mu_{water} + (1-\alpha)\mu_{air} \tag{5}$$

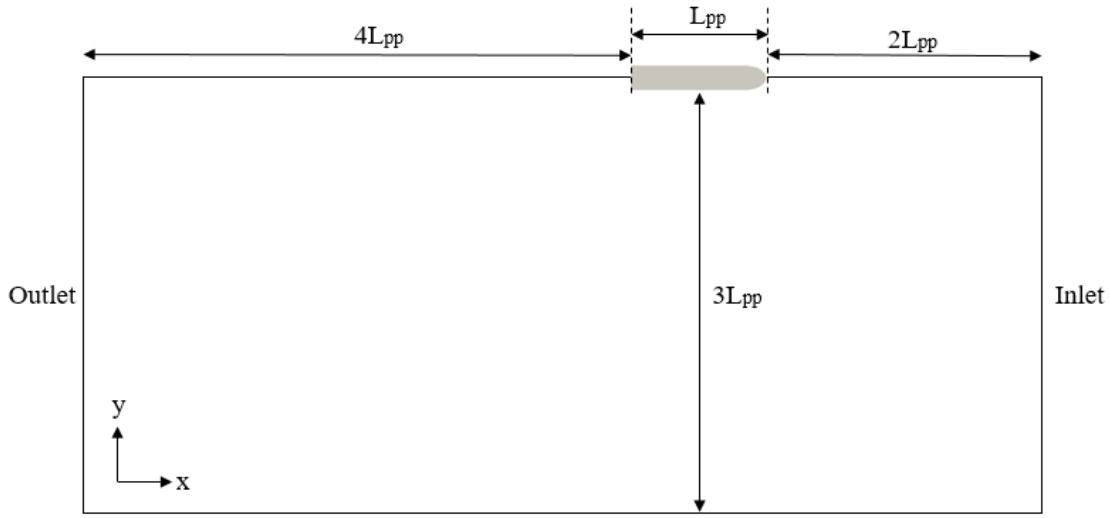

(a) Plan view; only half of the domain is shown but no symmetry plane condition is applied

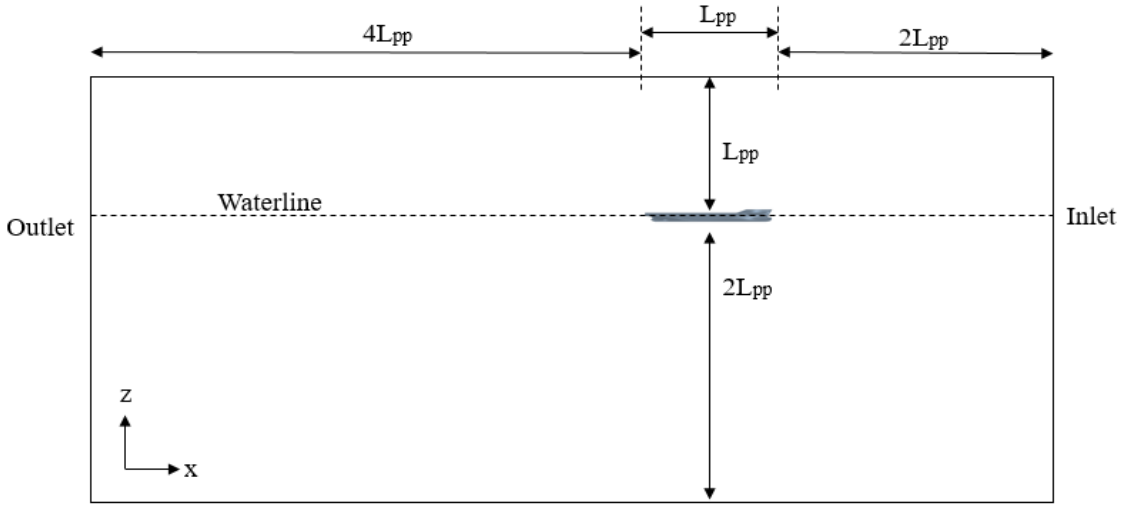

(b) Profile view

Figure 3: Illustration of the computational domain with dimensions.

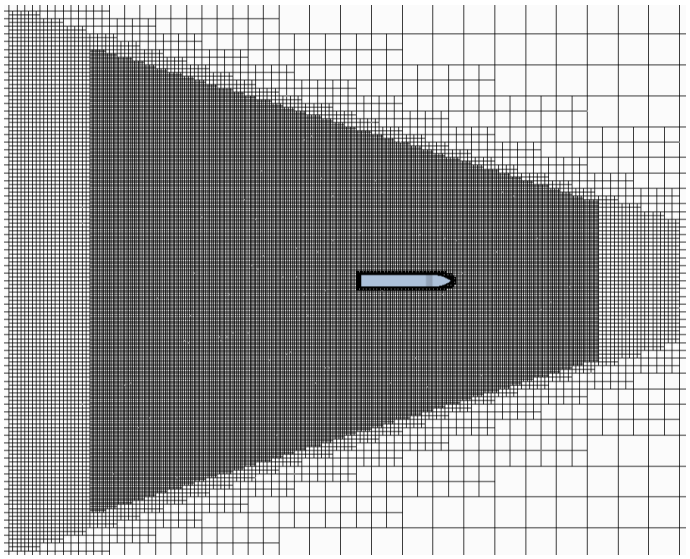

(a) Plan view

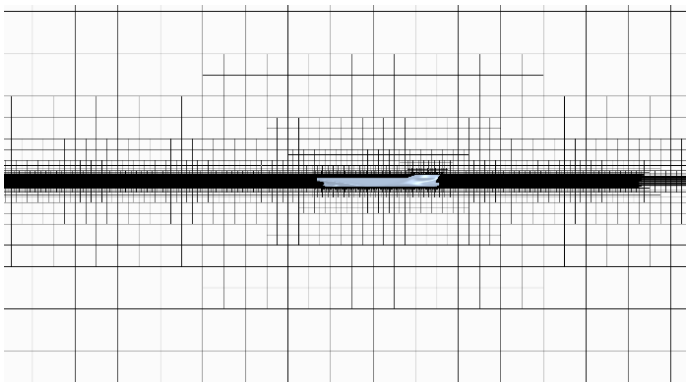

(b) Profile view

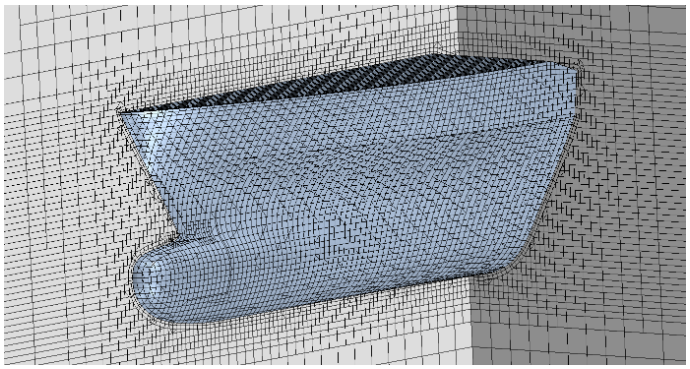

(c) Isometric view of bow region

Figure 4: Mesh layout of the model, in which local refinements are applied at the Kelvin-wave region, the free surface region and around the hull geometry.

2.2 DEM ice floes

Importing the ice floes is achieved by an array-injection method. The simulation first runs for a certain time without sea ice to allow the fluid domain to achieve a steady-state, i.e. when the ship wake become stable. Subsequently, an array of ice floes is injected into the computational domain near the inlet boundary, as shown in Figure 5(a). The ice floes are initialised to have the same velocity as the water flow ($U_{ice} = U_{water}$), and one ice floe array is injected to the same region every $t_{inject} = L_{array}/U_{ice}$, so that the next ice floe array can just follow the former one, as shown in Figure 5(b). Thus, the injection of ice floes does not influence the stability of solutions around the ship, and the ship can keep advancing in a continuous ice-floe zone, as desired, shown in Figure 6. With this method, an ice-floe route of unlimited length can be achieved without the need for a very long domain, which significantly saves computational costs.

The ice floes are modelled as DEM particles in the Lagrangian framework moving in the Eulerian fluid domain [46]. Each ice floe is modelled as a rigid thin disk, as in the present problem floes were principally pushed away by the ship rather than being deformed or broken up, as demonstrated by Polojärvi et al. [47]. The density of ice is set at ρ_{ice} = 900 kg/m^3, while ice diameter D and thickness h are variable. The movement of an ice floe can be considered as the combination of translation and rotation, which was solved with the rigid-body motion equations in the body-fixed system based on the mass centre of the floe G–$x'y'z'$:

$$\mathbf{F} = m\frac{d\overrightarrow{V_G}}{dt} \tag{7}$$

$$\mathbf{T} = [\mathrm{J}] \cdot \frac{d\overrightarrow{\omega_G}}{dt} + \overrightarrow{\omega_G} \times ([J] \cdot \overrightarrow{\omega_G}) \tag{8}$$

where **F** and **T** are the total force and torque on the ice floe, induced by the gravity, the hydraulic load from the surrounding fluid $\mathbf{F_h}$ and the contact force **Fc** from ship-ice contact and ice-ice contact; m and [J] are the mass and inertia moment tensor respectively, and V_G and ω_G are the translational and rotational velocity vectors of the ice floe respectively.

The hydraulic force $\mathbf{F_h}$ can be calculated based on the solution from the fluid domain, as expressed in Equation (9). Specifically, each DEM ice floe is projected into the fluid mesh, so that the cells around the floating disk are partially blocked by the disk volume and fluid solutions are interpolated on the disk surface, i.e. the fluid solution is integrated over the surface of each ice floe to contribute the total force and torque. Therefore, the cells around the free-surface area should be small enough to capture the floe geometry; Based on a preceding mesh study of wave force on a circular floating ice floe [30], at least 4

cells per ice thickness is applied in this study, and this needs to be refined accordingly when thinner ice is investigated. The timestep size used in CFD is 0.01 s to fulfil the condition that the Courant number (Co) is less than one, according to Equation (10). Each CFD timestep is split into 1000 DEM sub-timesteps so that the collisions can be sufficiently solved, which shows DEM dominates the time requested for the CFD+DEM computation.

$$\boldsymbol{F_h} = \int (-\overline{p}\,\boldsymbol{n} + \overline{\tau}\cdot\boldsymbol{n})\, dS \tag{9}$$

$$\mathrm{Co} = \frac{\mathrm{u}\Delta\mathrm{t}}{\Delta\mathrm{x}} \tag{10}$$

where $\Delta\mathrm{t}$ is the CFD timestep size, $\mathrm{u}/\Delta\mathrm{x}$ is its normal velocity divided by the distance between the cell centre and the centre of the neighbour cell.

The CFD+DEM is a one-way coupling mechanism, i.e. the ice movement does not provide feedback to the fluid domain, thus the wave radiation is not influenced by the floes. Two-way coupling is not chosen in this paper since it would induce very high computational costs. Also, the wave radiation mainly influences the floes moving away from the ship, so it is deemed to have little influence on the ship performance, as far as the ice concentration is not high enough to produce considerable wave reflection. The validation in Section 3.1 shows that the one-way mechanism is sufficient to provide accurate resistance predictions when ice concentration is up to 70%. In addition, Mucha [48] and Luo et al. [49] compared one-way and two-way CFD+DEM simulations for ship operations in brash ice channels; both reported that using two-way coupling did not make a notable difference on ship resistance predictions.

The contact force $\mathbf{F_c}$ is calculated by a penalty method [50], where ship/ice and ice/ice are allowed to have an overlap, according to the motion solutions. The overlap is modelled as a linear spring-dashpot system where the spring (k) accounts for the elastic response and the dashpot (η) reflects the energy dissipation during the contact, by which the normal and tangential components of $\mathbf{F_c}$ are calculated according to Equation (11) and (12) respectively. Subsequently, the contact force pushes the overlapped bodies apart so that the overlap is minimised in the final solution.

$$\mathbf{F_n} = -kd_n - \eta v_n \tag{11}$$

$$\mathbf{F_t} = \begin{cases} -kd_t - \eta v_t\,, & if\ |d_t| < |d_n|\mathrm{C}_f \\ |kd_n|\mathrm{C}_f \cdot \boldsymbol{n}\,, & if\ |d_t| \geq |d_n|\mathrm{C}_f \end{cases} \tag{12}$$

where d_n and d_t are overlap distances in the normal and tangential directions respectively, v_n and v_t are the normal and tangential components of the relative velocity between two contact bodies, C_f is the friction coefficient, which is set at 0.35 for ice-ice contact and 0.05 for ship-ice contact; k is set at 6×10^4 N/m and $\eta = 2C_{damp}\sqrt{kM_{eq}}$, in which C_{damp} is set at 0.067 and M_{eq} is the equivalent mass of two contact bodies, calculated as $M_{eq} = M_A M_B/(M_A + M_B)$. These parameter values are selected based on [11,51], and a slight adjustment was applied following a comparison with experimental results.

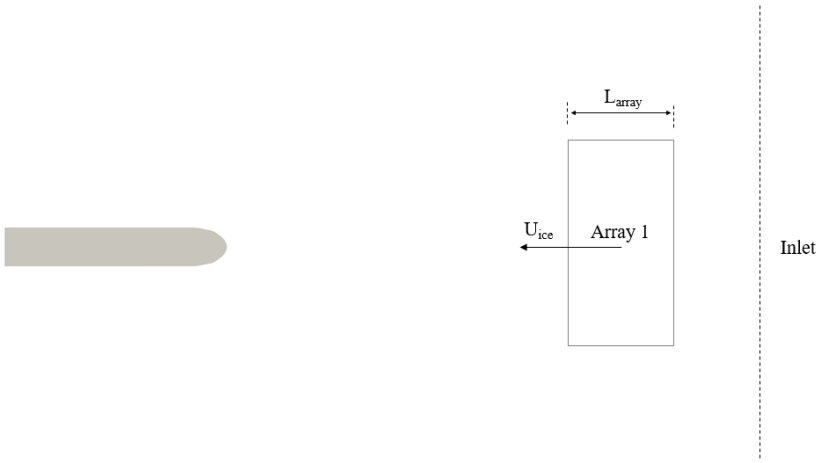

(a) $t = t_1$ when the first ice array is injected

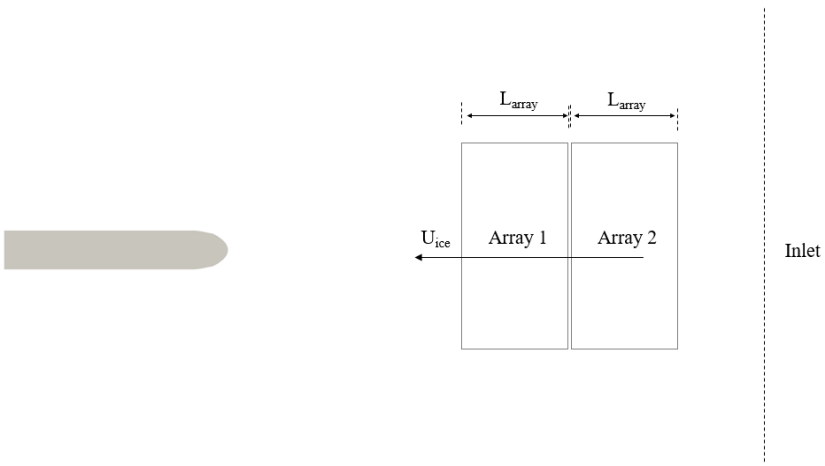

(b) $t = t_1 + t_{inject}$ when the second ice array is injected

Figure 5: Illustration of how ice floes are imported.

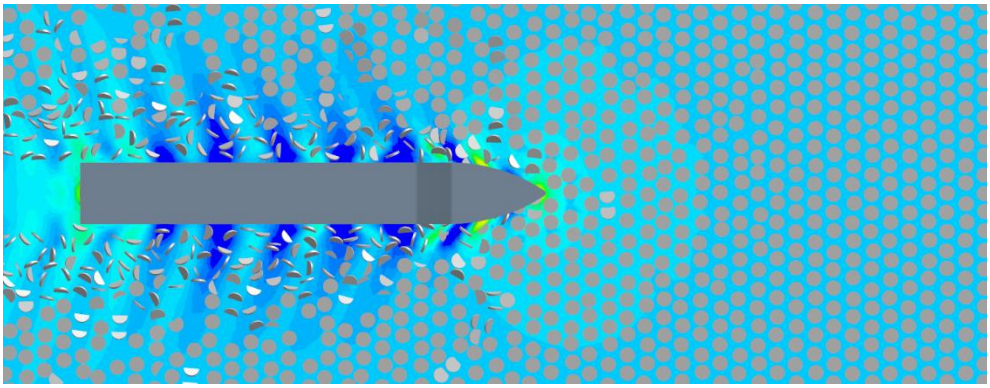

Figure 6: Simulation view of a ship advancing in floating ice floes.

2.3 Floe-distribution algorithms

The ice-floe array initialises floes to be of uniform size and equidistant to each other, as shown in Figure 6, which is not a realistic condition and introduces artificial regularity into the ice load. For example, such setup makes ship-ice contacts always occur at the same locations on the hull, which strongly dictates the resistance as well as structural response of the ship. This defect motivates the development of appropriate Floe-Size-Distribution (FSD) algorithms to introduce ice floes into a computational model where floe size and location can follow natural conditions observed in polar regions.

There are two principal features for realistic FSD: (a) ice floes are a mixture of different sizes, and (b) the location of each ice floe should be randomly distributed. The distribution of floe size against possibility is suggested to follow a log-normal function [4], an example is shown in Figure A1. For this purpose, two algorithms have been developed to generate a natural ice-floe map within a desirable domain. Main inputs of both algorithms are the length and width of the domain, as well as the ice concentration (C), defined as the ice-covered area divided by the whole sea-surface area, i.e. area of the domain. There are two constraints for the proposed problem: the first one is to avoid overlapping between ice floes, and the other is to assure that the centre of every floe lays inside the domain boundary. In this study, the thickness of all floes is assumed to be consistent.

Algorithm (I) first calculates the number of ice floes and marks them from 1 to n_p, and then it randomly injects all ice floes inside the domain and their initial locations are stored in a location matrix. Subsequently, the algorithm proceeds by considering every piece separately, starting from i=1 to i=n_p. The algorithm first checks if overlapping occurs (with other ice pieces and with the boundary of the domain). Where an overlapping occurs, the vicinity of the ice piece is searched to see whether there is a sufficient space for it to move over (direction vector revolves 360 degrees and searches the space in the vicinity of the original position). If there is sufficient space in the vicinity, the ice floe will be moved there, and the location matrix is updated. If there is not enough available space in the vicinity, the ice

289 piece is then randomly reallocated to another position. The process iterates until all ice pieces are settled
290 and no constraints are violated, depicted in Figure A2.

291 Algorithm (I) is able to rapidly yield ice distributions up to C = 60%. Nevertheless, it gets slower for
292 higher C values, since this means there is less open-water space in the domain and thus it is harder to
293 move the floes into free space. Therefore, in order to deal with high-concentration ice conditions,
294 Algorithm (II) has been developed. It is based on the Genetic Algorithm (GA) [52], which is an
295 optimisation technique inspired by Darwin's principles of the survival of fittest individuals. Algorithm
296 (II) defines a penalty factor to indicate the overlapping between ice floes, where a higher penalty value
297 corresponds to a higher overlapping area. The target penalty factor is set to be zero in this study,
298 meaning no overlapping at all. In other words, the target penalty factor can be set to be larger than zero
299 when certain ice overlapping is allowed, which is suitable for modelling ice herding and rafting [13,53].

300 To initialise Algorithm (II), a certain number (M_0) of parent distributions are randomly obtained,
301 corresponding to M_0 penalty factors. Subsequently, the algorithm selects a small number of solutions
302 (M_1) with the lowest penalty factors, which will be used as parents to produce child distributions,
303 yielding the same overall amount of M_0 solutions for the next generation. Namely, only fittest
304 individuals survive, while the rest of them are discarded by the algorithm. Thus, the average of selected
305 solutions is better than the previous ones, leading to a higher probability to get better child solutions. In
306 addition, M_2 best solutions, known as elite individuals, automatically survive to the next generation
307 without a change; while the rest of the solutions ($M_1 - M_2$) relocate ice floes to get ($M_0 - M_2$) new
308 distributions, which are combined with the elite individuals to form the next parents. Iterations are
309 performed until one distribution has been found to achieve the targeting penalty factor, as portrayed in
310 Figure A3. In this study, $M_0 = 2000$, $M_1 = 1000$ and $M_2 = 100$.

311 Algorithm (II) is slower compared to (I) to obtain a desired solution, while it is capable of generating
312 high-concentration floe fields. The output from both algorithms is a matrix listing the *x*-*y* coordinates
313 of every ice piece and the corresponding floe size, while *z* coordinate is aligned to the buoyancy-gravity
314 equilibration of each floe. Figure 7 shows two samples of floe distributions obtained by algorithms (I)
315 and (II) respectively, where the targeted FSD and C are exactly achieved. The FSD can be easily
316 switched to any field measurements or aerial observations, such as [3,54]. Moreover, although the shape
317 of ice floes was set to be circular to fit the pancake-ice nature, both generators are capable of modelling
318 other ice shapes. The algorithms aspire to replicate the polar floe features as much as possible, while
319 the results are still not perfectly natural, e.g. real pancake ice can be elliptical, close to circular but not
320 exactly circular.

321 For a specific FSD and C condition, the algorithms can generate the corresponding ice field for a ship
322 to enter, which is used to replace a regular array as in Figure 6. Updated simulations are shown in Figure
323 8, in which the artificial regularity of ice load has been avoided. Up to this point, the computational

modelling for the present work is completed. Noting that the introduced algorithms are not only compatible with current work, they are also useful for other polar modelling involving ice floes.

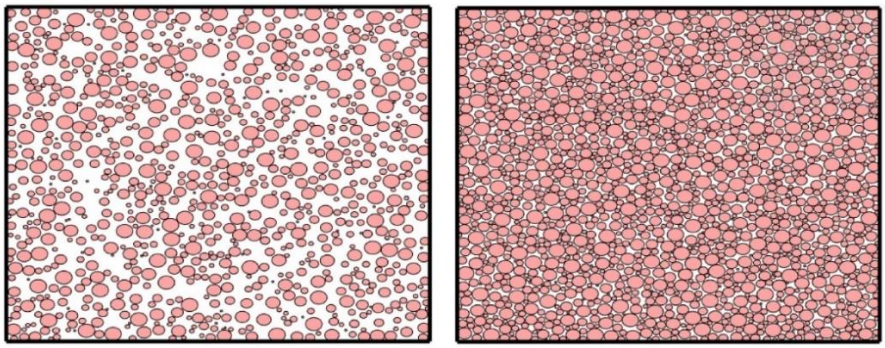

Figure 7: Ice-floe fields obtained by Algorithm (I), C = 40% (left side); and by Algorithm (II), C = 70% (right side).

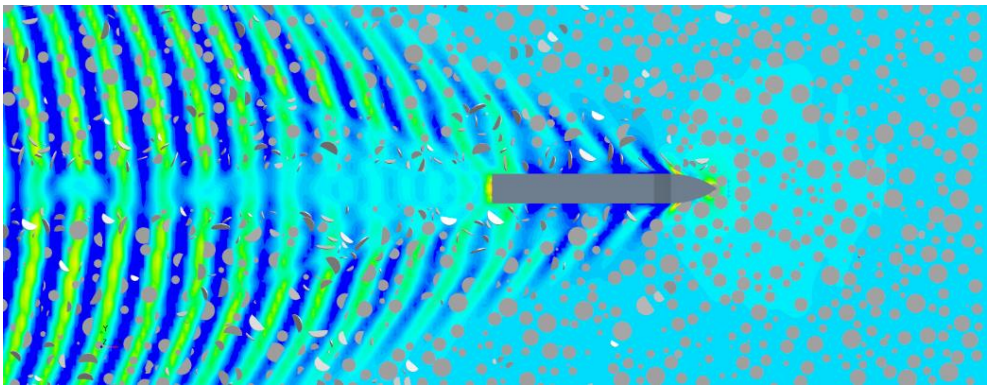

(a) Ice concentration = 30%

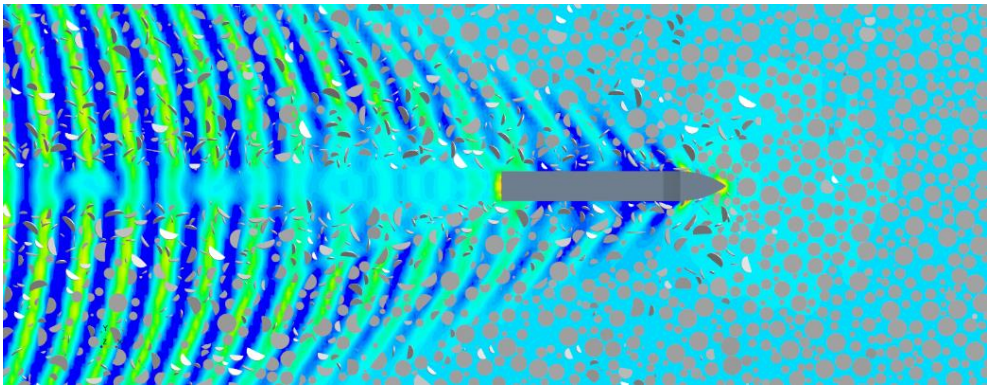

(b) Ice concentration = 50%

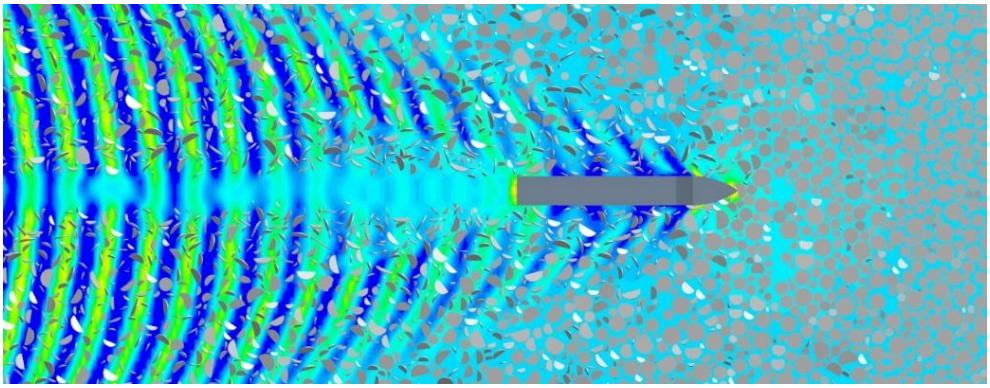

(c) Ice concentration = 70%

Figure 8: Simulation view of a ship advancing in floating ice floes, with natural floe fields implemented.

3. Ship resistance

The predicted steady-state simulations are shown in Figure 8: when a ship is advancing in ice floes, ship-ice collisions occur at the bow area, causing the floes to be pushed aside and rotate within the wake, and in some cases, floes can slide along the ship before being pushed away. This work focuses on the ship resistance, namely the force born by the ship in its advancement direction, since this determines the power required for such shipping. The total resistance of the ship consists of an ice resistance R_{ice} induced by the floes and a water resistance R_{water} similar to an open-ocean case ($R_{total} = R_{ice} + R_{water}$). R_{ice} occurs due to ship-ice collisions at the bow area as well as the force due to floe sliding. It is calculated by summing of ship-ice contact impulses in the *x*-direction over a certain time period and then dividing the total impulse by the time. An example of the impulse time-series is shown in Figure 9, where the varying values correspond to ship contacts with floes of different sizes. Randomness can be seen in the time-series, which is reasonable due to the nature of the floe-distribution algorithms. Therefore, before taking a resistance result, each simulation needs to be run for a sufficiently long time (more than 40 s) to offset this randomness, i.e. until R_{ice} does not noticeably change with runtime, as shown in Figure 10. Every 40 seconds of the CFD&DEM simulation costs approximately two days in real time using a 100-core High Performance Computation (Intel Xeon E5-2630v3).

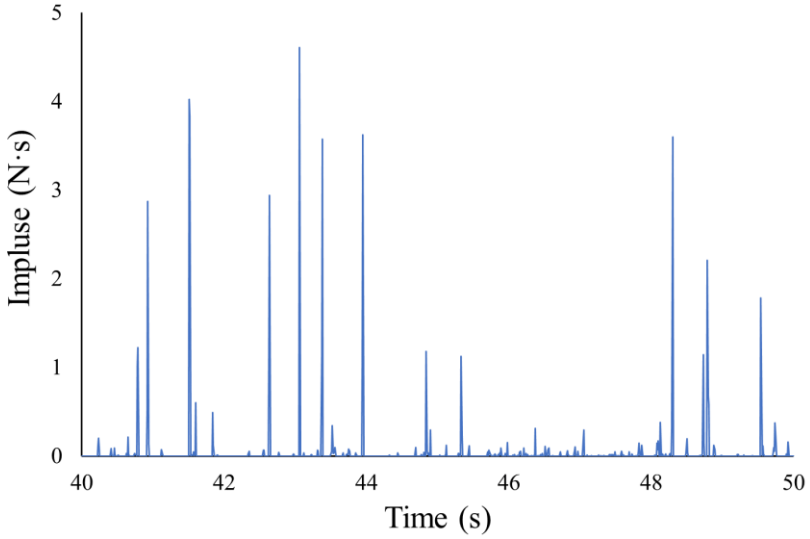

Figure 9: Time series of ice-induced impulse against the direction of ship advancement (obtained when Fr = 0.12, C = 60%, *h* = 0.02 m and FSD follows [4]).

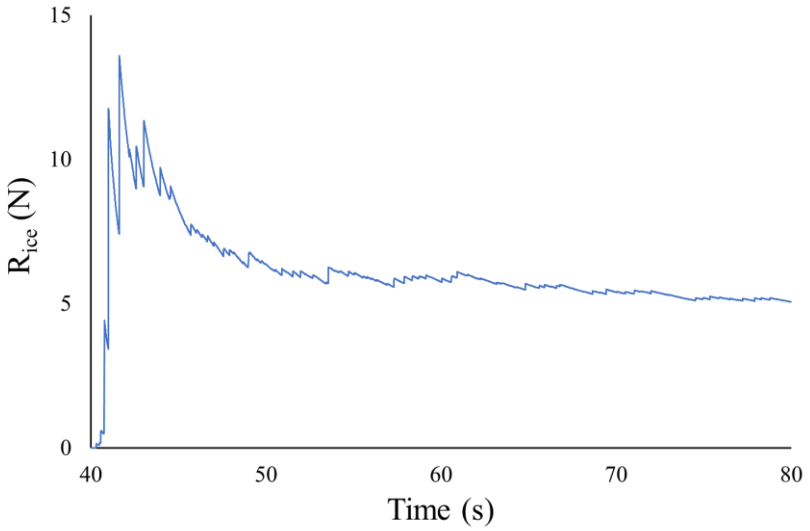

Figure 10: Time series of ice resistance: an oscillation is shown when the ship just enters the floe field, and then R_{ice} approaches a steady value over time.

3.1 Validation

The predicted resistance has been validated against the experiments conducted in the towing tank of Harbin Engineering University [4]. The computational resistance is compared with available experimental data, where ship speeds ranged from Froude number Fr = 0.06 to 0.18, and ice concentration C = 60% and 70%, ice thickness *h* = 0.02 m. The comparison between computational and

experimental results is presented in Figure 11, and the good agreement indicates a reliable accuracy of the model in predicting ship resistance in ice floes. Figure 11 also shows the open water component, and R_{ice} can be seen as the difference between the total-resistance curve and the water-resistance curve. This work only considers ice concentrations of up to 70%, since ice rafting may occur with higher concentrations (when C > 79% according to the result of Hopkins and Tuhkuri [11]), while the capability of introduced CFD&DEM approach on modelling ice rafting needs further verifications, where the floe contact is between surfaces rather than edges.

Despite the good agreement between the resistance curves from the experiments and simulations, it is important to note that there are certain differences between the experiment and the simulation. Firstly Guo et al. [4] applied square shapes of ice, while in the present study the ice was defined to be circular. The reason for this is that the circular ice is closest to the potential Arctic nature; also, in the DEM method, simulating square ice would be more computationally time-consuming than circular, meaning it would be challenging to run a sufficiently large number of simulations to determine the relationships of ice resistance with principal environmental variables. Appendix B provides a supplementary study to show the shape difference does not cause large uncertainness in this work. Secondly, the ship heave and pitch were enabled in the experiments, but it is not included in the simulations since both motions were reported to be negligible in the experiments with the calm water condition applied. Beyond these two points, the simulations have realistically replicated the experiments. Other parts of the model setup, particularly the mass of each floe and the FSD, have been matched.

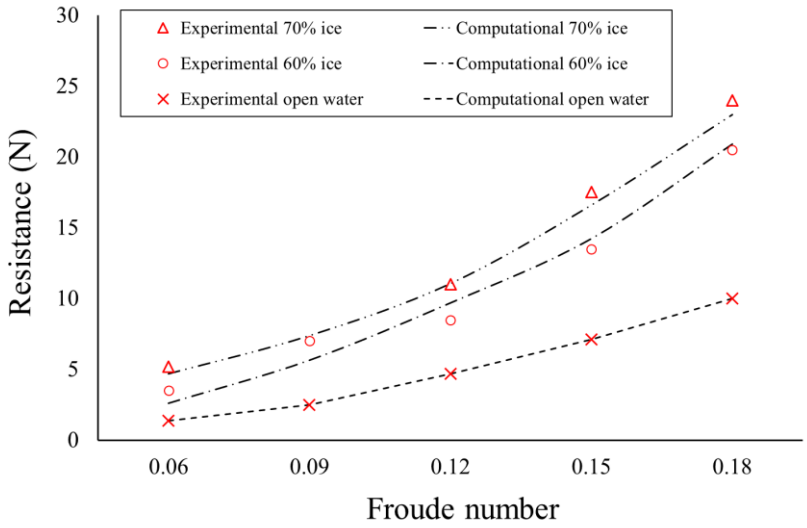

Figure 11: Experimental [4] and computational total resistance of model-scale KCS operating in ice concentration 60% and 70%, alongside the water component.

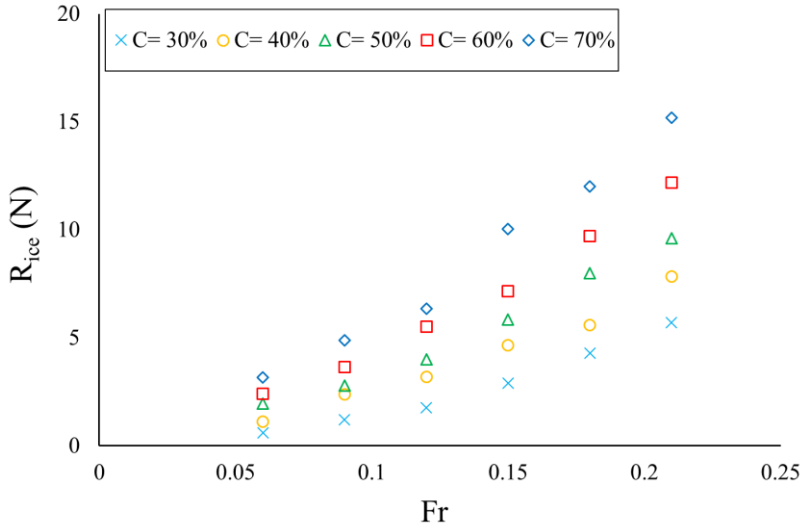

(a) Ice resistance values

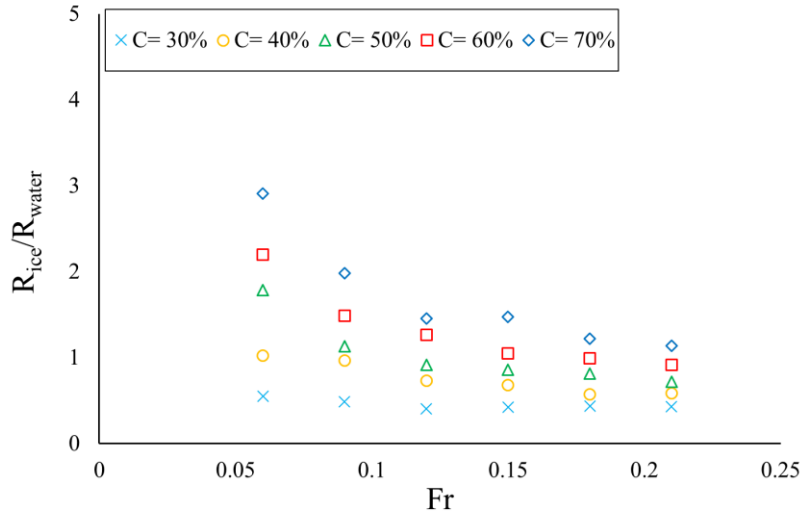

(b) Ice resistance normalised by water resistance

Figure 12: Ice-floe resistance in varying ice concentrations and ship speeds.

3.2 Ship speed and ice concentration

Extended simulations were performed to investigate the influence of ship speed and ice concentration. Figure 12 presents the ice resistance for varying ship speeds and ice concentrations. Figure 12(a) shows the variation trend of R_{ice}; regression analyses indicate that the increasing powers of ship speed and ice concentration are around 1.2 and 1.5 respectively in the examined range. Thus, the increase of R_{ice} with an increasing ship speed is slower than that of R_{water} whose power is recognised to be 2. Figure 12(b) presents the ratio of R_{ice} to the corresponding R_{water}, indicating the ice-induced resistance increments in

the specific conditions, important for powering and fuel estimates. The ratio is higher when the ship is relatively slow; this is because R_{ice} increases more slowly than R_{water}, also it could be affected by ship-generated waves which tend to push the floes away and reduce the ship-ice contact, as it is stronger with a faster ship.

To distinguish the effect of ship-generated waves, comparisons were made between simulations with and without waves enables, as illustrated in Figure 13. This clearly shows the wave can push the floes away from the hull, while when waves are eliminated, floes slide closely along the hull and present more contacts. The wave-reduced ship-ice contacts reflect in a reduced $R_{ice,}$ as shown in Table 2. The reduction in R_{ice} takes up around 30% in a range of velocities, i.e. considerable but not dictated by wave strength, which means this effect is essentially about avoiding contacts, rather than how far the floes are pushed away. Figure 14 displays, when the wave is ignored, R_{ice}/R_{water} decrease is slower with increasing ship speed; this difference corroborates that the wave effect will be more evident with a faster ship.

As waves are shown to significantly influence the ship-ice interaction and ice resistance, it corroborates the importance of the inclusion of CFD flow in the present work. Since previous sole-DEM work reported inaccuracies in certain ranges, it can now be deduced that those inaccuracies may result from the negation of waves; by contrast, the R_{ice} curves from the current CFD&DEM approach demonstrated to be accurate in the whole examined range. Nevertheless, it should be noted the simulations are conducted at model scale; in full scale the floes may not be pushed away to the same extent: the mass of the floes scales as D^3, but the forces due to waves are known as scaled by D^2, where D is floe diameter.

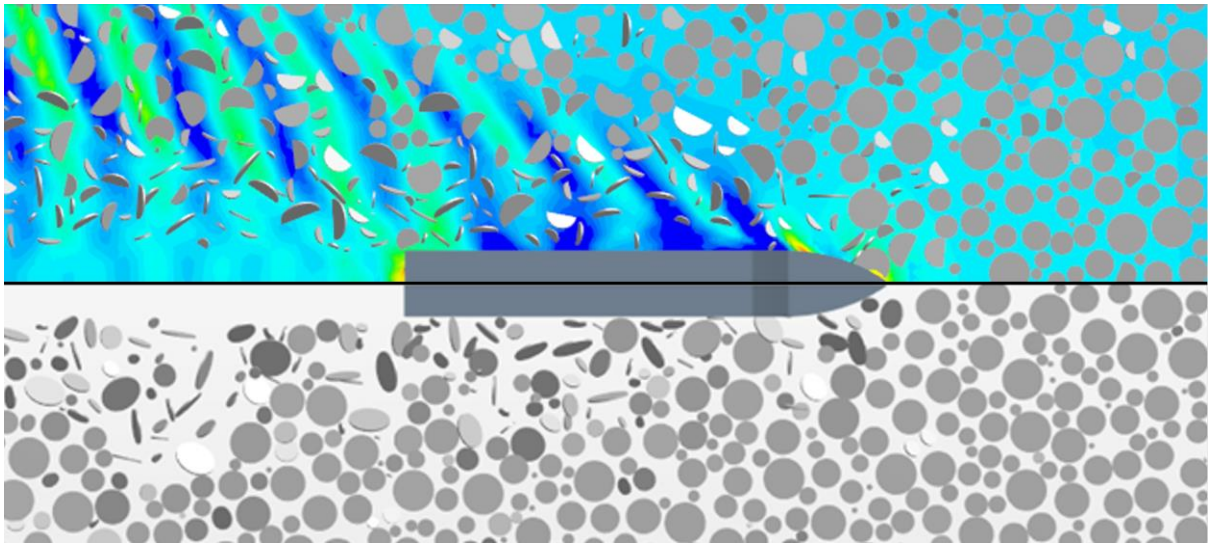

Figure 13: Comparison between ship-ice interactions with and without waves.

Table 2: Comparison of ice resistance between with & without ship-generated waves, when C = 60%.

	Fr = 0.06	Fr = 0.12	Fr = 0.18
R_{ice} with wave (N)	2.40	5.52	9.70
R_{ice} without wave (N)	3.50	8.31	14.49
Relative reduction by the wave (%)	31.4%	33.5%	33.0%

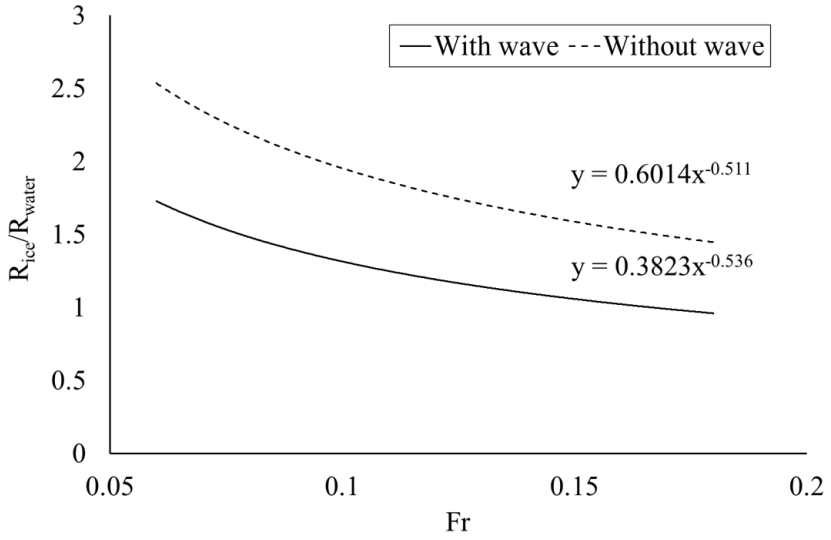

Figure 14: Comparison of R_{ice}/R_{water} between with & without ship-generated waves, when C = 60%. Regression powers display that R_{ice}/R_{water} reduces more slowly when waves are ignored.

3.3 Floe diameter and ice thickness

The influence of floe diameter is analysed by globally scaling all floes, i.e. multiplying the FSD curve with a factor. Figure 15 compares varying floe-diameter conditions while ice concentration remains constant. It can be seen that larger floe diameters lead to sparser ice (fewer floes) and lower the collision frequency, while significantly increasing the peak impulses. The overall ice resistance with different floe diameters are plotted in Figure 16, in which the resistance evidently increases with increased floe diameters; despite a lower collision frequency, the force integration over time still increases due to the peak values. This indicates that, with the same ice concentration, the effect of floe diameter on ship resistance is more dominant than that of collision frequency. Overall, R_{ice} reveals a linear trend with varying floe diameter.

The influence of ice thickness on the resistance is studied by varying *h* while keeping other parameters constant. Figure 17 presents the ice resistance when *h* = 0.004 – 0.02 m, and for C = 40% and 60%. Similar to floe diameter, R_{ice} reveals a linear trend with varying ice thickness. When FSD and C are held

constant, varying *h* can also be considered as varying the mass of each floe, thus total ice mass ($\sum m_{ice}$) is varied according; In another study on ship interaction with ice ridge, Gong et al. [55] reported a similar quasi-linear relationship between $\sum m_{ice}$ pushed by a ship and the corresponding ice resistance. However, in Figure 12, $\sum m_{ice}$ changes linearly with ice concentration, while R_{ice} changes at power of 1.5; and in Figure 15 and 16, $\sum m_{ice}$ remains constant when floe diameters are changed, while $\sum m_{ice}$ apparently changes. This indicates it cannot conclude that ship resistance varies linearly with $\sum m_{ice}$ in this ice-floe scenario, since waves and FSD have introduced complexities into the problem. Each variable needs to be analysed separately in this case.

4. Conclusions

A CFD&DEM approach has been introduced simulate a ship advancing in floating ice floes, since such a condition has been predicted to be the main navigation environment of future Arctic shipping. Relevant numerical theories and practicalities have been presented in detail: CFD is incorporated with DEM to model desirable ship-wave-ice interactions, and two algorithms for generating natural ice-floe fields have been provided. The proposed model shows the capability to simulate and analyse the proposed problem with high fidelity, and it is validated to be accurate in predicting the ship resistance induced by ice floes. A series of simulations have been performed to investigate how the ice resistance is influenced by ship speed, ice concentration, ice thickness and floe diameter. It was found that ship speed and ice concentration govern the resistance with a power of 1.2 and 1.5 respectively, whilst floe diameter and ice thickness both show a linear effect. These relationships will be useful to derive empirical equations to provide rapid estimates for ship resistance in this emerging environment – floating ice floes.

This work presents the first model that includes CFD flow to account for ship-generated waves in the ship-wave-ice interaction process, which proves to be of great importance: the wave evidently reduces the ship-ice collisions and is proved as an essential factor in predicting the resistance from floating floes. Future work should consider extended scenarios where ice cracking or facture cannot be ignored, for which, the present code may be developed by bonding multiple DEM particles together to form one ice piece while setting appropriate criteria that trigger these bonds to break [56].

Acknowledgements

This work is part of a project that has received funding from the European Union's Horizon 2020 research and innovation programme under grant agreement No 723526 - SEDNA: Safe maritime operations under extreme conditions; the Arctic case. The first author is grateful to Lloyds Register Foundation, UCL Faculty of Engineering Science and China Scholarship Council, for providing his

PhD scholarship; he appreciates the ongoing support of Professor Guoxiong Wu. The authors acknowledge the use of the UCL Grace High Performance Computing Facility (Grace@UCL), and associated support services, in the completion of this work.

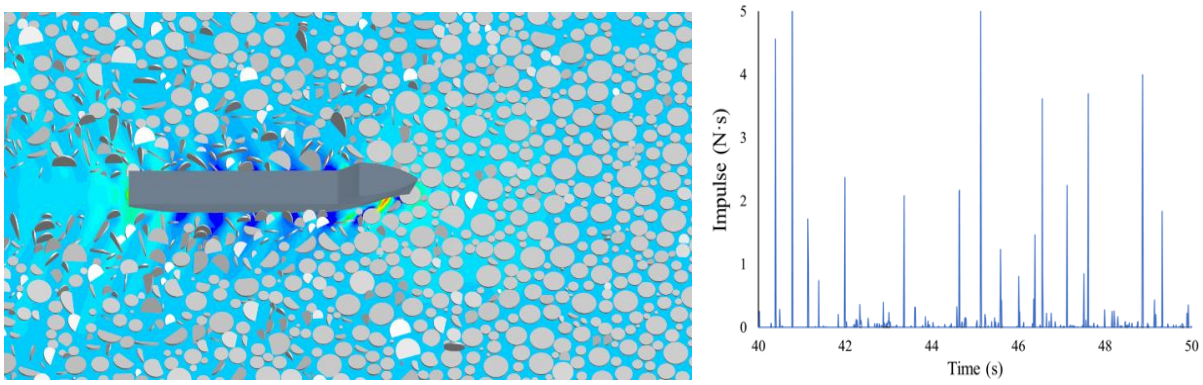

(a) Floe diameters are the same as those in [4]

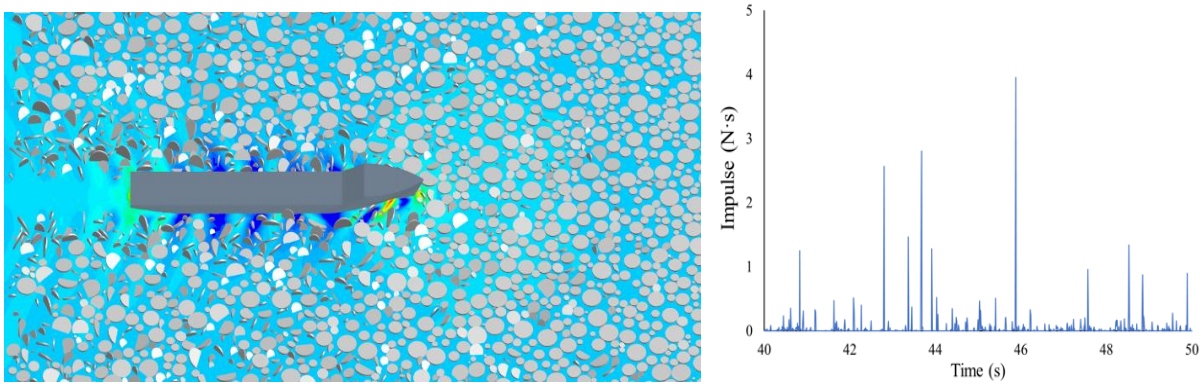

(b) Floe diameters are 60% of those in [4]

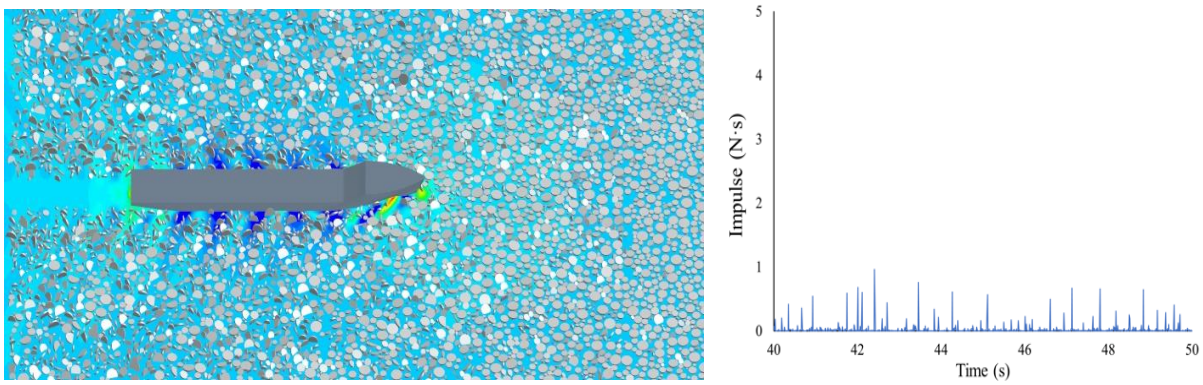

(c) Floe diameters are 20% of those in [4]

Figure 15: Ship advancing in different-sized floes (left side) and corresponding time-series of resistance impulse (right side); obtained when Fr = 0.15, h = 0.02 m and C = 60%.

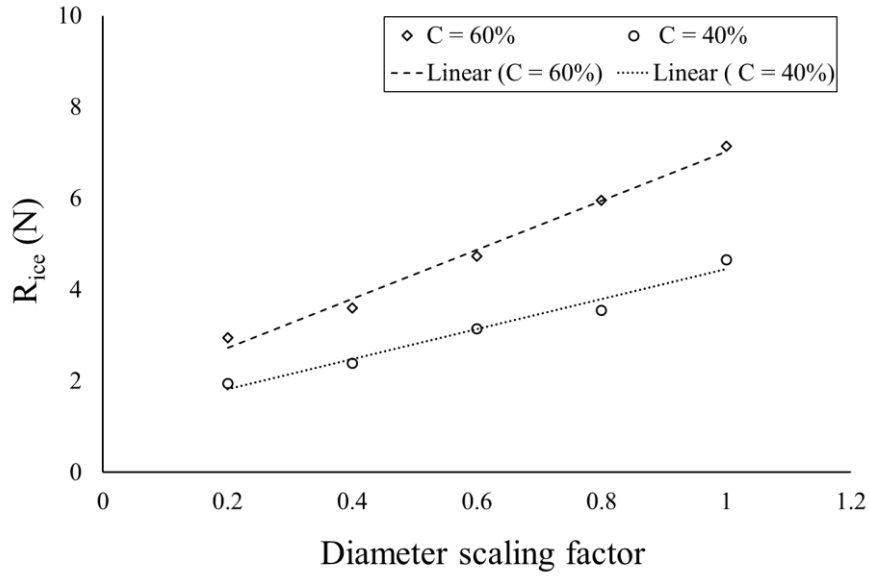

Figure 16: Ice-floe resistance in different-sized floes (floe diameters of [4] globally scaled by a factor), obtained when Fr = 0.15 and h = 0.02 m.

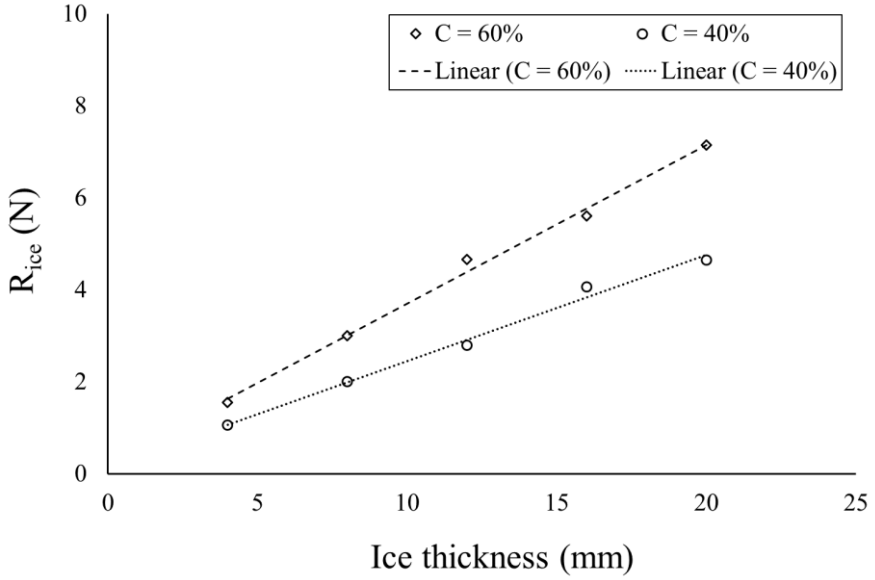

Figure 17: Ice-floe resistance in varying ice thicknesses, obtained when Fr = 0.15.

Appendix A: Supplementary material for the floe-distribution algorithms

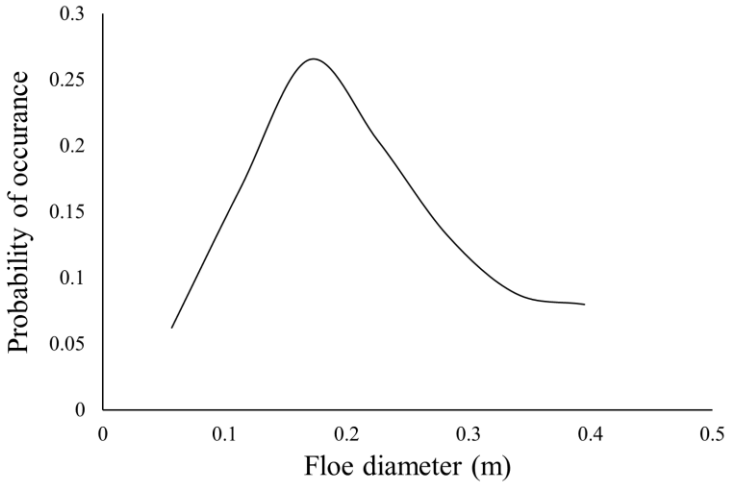

Figure A1: FSD curve example, in which the surface area of each floe is as per Guo et al. [4].

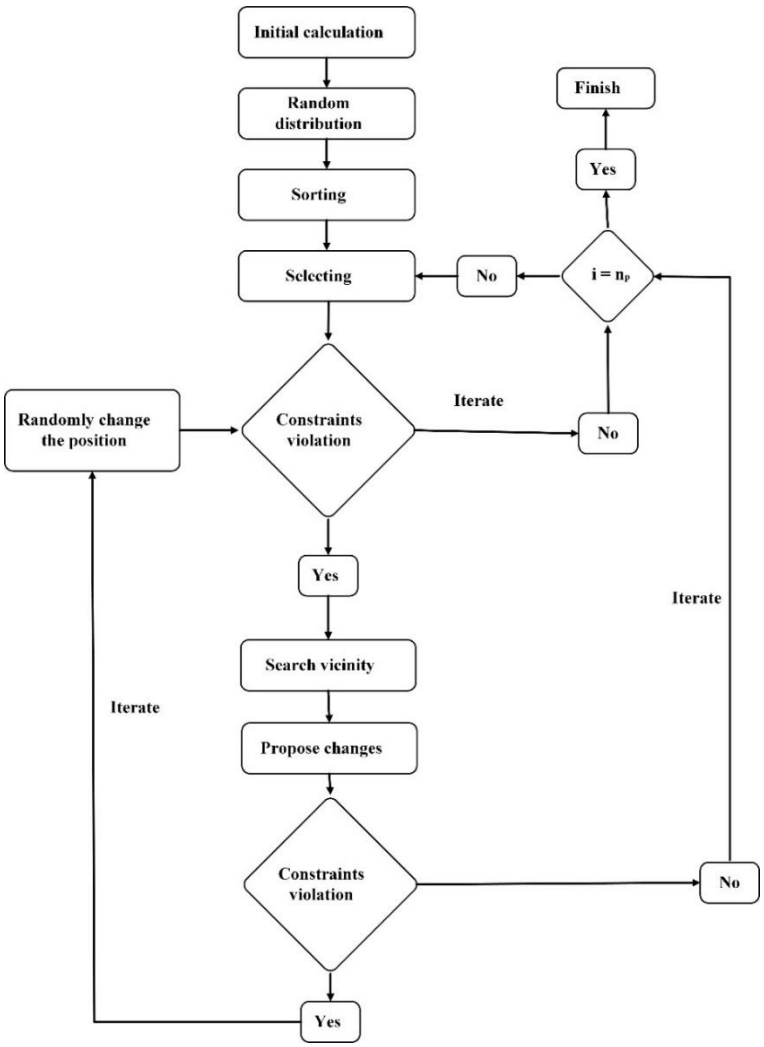

Figure A2: Flow chart of Algorithm I.

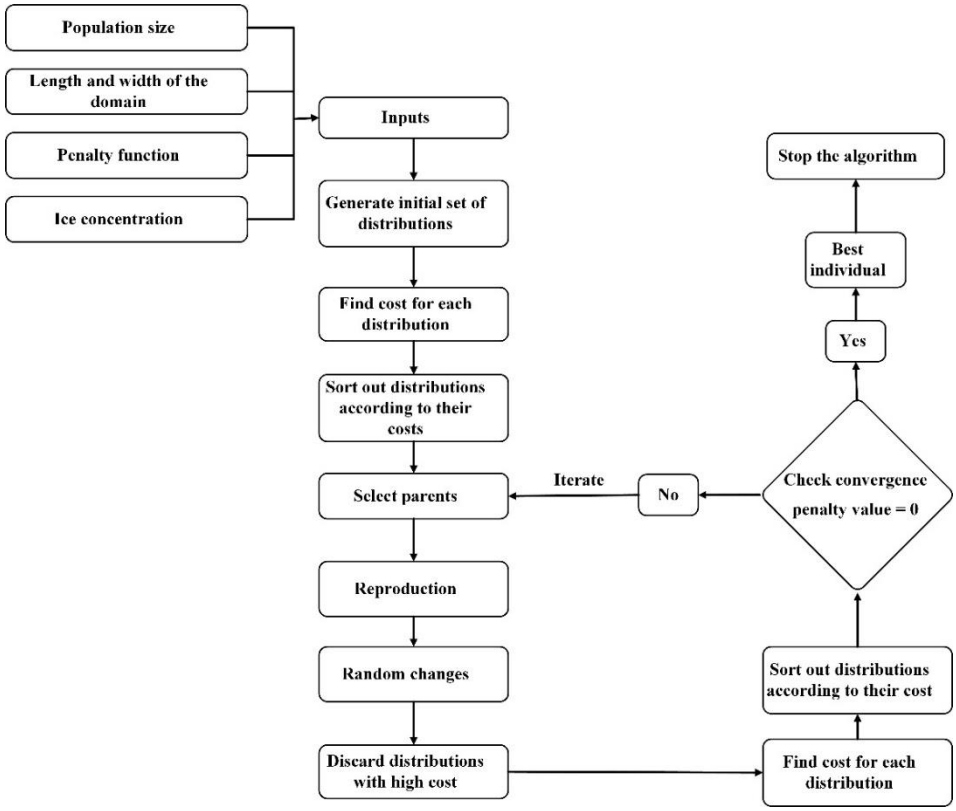

Figure A3: Flow chart of Algorithm II.

Appendix B: Comparing the loads on a ship bow between square and circular ice.

This appendix introduces a brief analysis on the influence of ice shape on ship resistance. A simplified test was conducted in which one piece of ice colliding with the KCS bow in different scenarios: (a) circular ice (b) square ice with a flat side towards the bow (c) square ice with a sharp edge towards the bow; as shown in Figure B1. This simplified setup can provide valid representation for the simulations in the main text, where each ship-ice collision occurs mostly between the ship and a single floe, as shown in Figure 8. In the three scenarios, the ship speed, ice surface area and ice thickness are the same, in which the surface area is taken as the median value of the experiment for validation [4]. The corresponding ice loads are listed in Table B1.

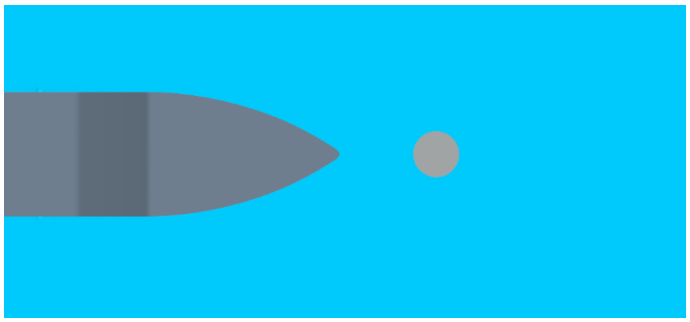

(a) circular ice

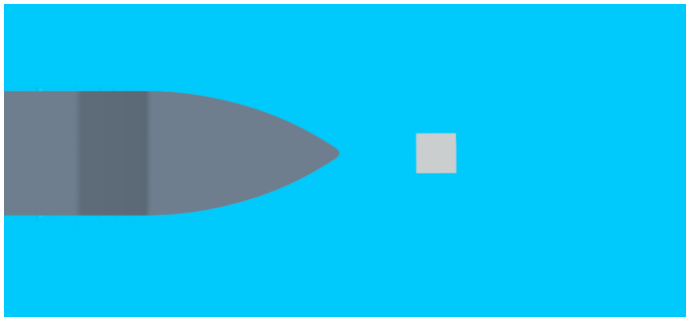

(b) square ice with the flat side towards the bow

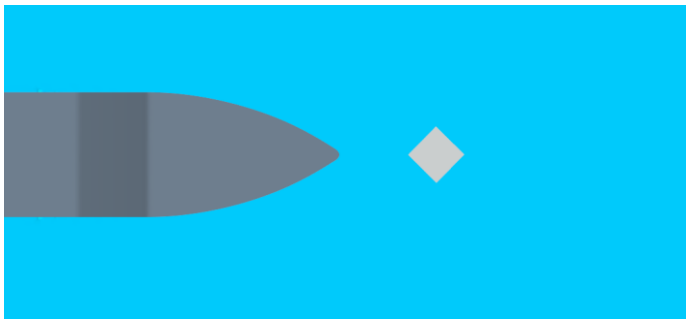

(c) square ice with the sharp edge towards the bow

Figure B1: Ship advancement to make contacts with ice in different shape scenarios.

Table B1: Ice loads obtained from different shape scenarios, Fr = 0.12.

	Circular ice	Square ice with a flat side towards the bow	Square ice with a sharp edge towards the bow
Ice-induced impulse against the direction of ship advancement (N*s)	16.49	16.35	17.47

The results have shown scenarios (a) and (b) cause a similar ice load, and the shape would cause a difference between scenarios (a) and (c), although it is less than 10%. For circular ice, the ice load is the same regardless which side is encountered by the ship; for square ice, the ice load is subjected to the contact angle, which should lay in a spectrum between scenarios (b) and (c). In the main text of this paper, the ship resistance is a statistical result from a sufficiently large number of floes and a sufficiently long operation time, thus the uncertainness caused by shape difference would be less than 10% too. This agrees with small deviations shown in Figure 11 and supports the reasonable adjustment of the ice shape to obtain findings based upon a more realistic ice condition.

However, this conclusion cannot be taken as that ice shape is not important in ship-ice interactions; it is based on certain features in this work:

(i) Ice floes are modelled as rigid in both the simulation and experiment. In reality, the ice could fracture especially in scenario (c), which would cause a different load.

(ii) The ship speed is relatively fast ($0.06 < Fr < 0.21$), so the ice response is mainly bouncing away, rather than continuous contacts with the ship. In a slow speed condition (usually for ice-structure interactions, considering ice drift speed and a static structure, $Fr < 0.02$), the shape difference would be more influential [57].

(iii) This study limits C to be no more than 70%. With a higher C, a floe would be harder to be pushed away due to the obstacle of other floes; in such a situation, force chains between floes [58, 59] are likely to form, which can make the floe shape important for ship resistance [57].

References

[1] J. Thomson, S. Ackley, F. Girard-Ardhuin, F. Ardhuin, A. Babanin, G. Boutin, J. Brozena, S. Cheng, C. Collins, M. Doble, Overview of the arctic sea state and boundary layer physics program, Journal of Geophysical Research: Oceans. (2018).

[2] L.C. Smith, S.R. Stephenson, New Trans-Arctic shipping routes navigable by midcentury, in: Proceedings of the National Academy of Sciences, 2013: pp. E1191–E1195.

[3] A. Alberello, M. Onorato, L. Bennetts, M. Vichi, C. Eayrs, K. MacHutchon, A. Toffoli, Brief communication: Pancake ice floe size distribution during the winter expansion of the Antarctic marginal ice zone, The Cryosphere. 13 (2019) 41–48.

[4] C. Guo, C. Xie, J. Zhang, S. Wang, D. Zhao, Experimental Investigation of the Resistance Performance and Heave and Pitch Motions of Ice-Going Container Ship Under Pack Ice Conditions, China Ocean Eng. 32 (2018) 169–178. https://doi.org/10.1007/s13344-018-0018-9.

[5] W.-Z. Luo, C.-Y. Guo, T.-C. Wu, Y.-M. Su, Experimental research on resistance and motion attitude variation of ship–wave–ice interaction in marginal ice zones, Marine Structures. 58 (2018) 399–415. https://doi.org/10.1016/j.marstruc.2017.12.013.

[6] M.-C. Kim, W.-J. Lee, Y.-J. Shin, Comparative study on the resistance performance of an icebreaking cargo vessel according to the variation of waterline angles in pack ice conditions, International Journal of Naval Architecture and Ocean Engineering. 6 (2014) 876–893. https://doi.org/10.2478/IJNAOE-2013-0219.

[7] J.-H. Kim, Y. Kim, H.-S. Kim, S.-Y. Jeong, Numerical simulation of ice impacts on ship hulls in broken ice fields, Ocean Engineering. 180 (2019) 162–174.

[8] J. Tuhkuri, A. Polojärvi, A review of discrete element simulation of ice–structure interaction, Philosophical Transactions. Series A, Mathematical, Physical, and Engineering Sciences. 376 (2018).

[9] S. Løset, Discrete element modelling of a broken ice field—Part I: model development, Cold Regions Science and Technology. 22 (1994) 339–347.

[10] S. Løset, Discrete element modelling of a broken ice field — Part II: simulation of ice loads on a boom, Cold Regions Science and Technology. 22 (1994) 349–360. https://doi.org/10.1016/0165-232X(94)90020-5.

[11] M.A. Hopkins, J. Tuhkuri, Compression of floating ice fields, Journal of Geophysical Research: Oceans. 104 (1999) 15815–15825.

[12] M.A. Hopkins, H.H. Shen, Simulation of pancake-ice dynamics in a wave field, Annals of Glaciology. 33 (2001) 355–360. https://doi.org/10.3189/172756401781818527.

[13] M. Dai, H.H. Shen, M.A. Hopkins, S.F. Ackley, Wave rafting and the equilibrium pancake ice cover thickness, Journal of Geophysical Research: Oceans. 109 (2004).

[14] A. Herman, Wave-Induced Surge Motion and Collisions of Sea Ice Floes: Finite-Floe-Size Effects, Journal of Geophysical Research: Oceans. 123 (2018) 7472–7494. https://doi.org/10.1029/2018JC014500.

[15] A. Herman, S. Cheng, H.H. Shen, Wave energy attenuation in fields of colliding ice floes. Part A: Discrete-element modelling of dissipation due to ice-water drag, The Cryosphere Discussions. (2019) 1–21. https://doi.org/10.5194/tc-2019-121.

[16] A. Herman, S. Cheng, H.H. Shen, Wave energy attenuation in fields of colliding ice floes. Part B: A laboratory case study, The Cryosphere Discussions. (2019) 1–20. https://doi.org/10.5194/tc-2019-130.

[17] E.H. Hansen, S. Løset, Modelling floating offshore units moored in broken ice: comparing simulations with ice tank tests, Cold Regions Science and Technology. 29 (1999) 107–119.

[18] M. Lau, K.P. Lawrence, L. Rothenburg, Discrete element analysis of ice loads on ships and structures, Ships and Offshore Structures. 6 (2011) 211–221.

[19] S. Ji, Z. Li, C. Li, J. Shang, Discrete element modeling of ice loads on ship hulls in broken ice fields, Acta Oceanologica Sinica. 32 (2013) 50–58.

[20] J. Wang, A. Derradji-Aouat, Ship performance in broken ice floes-preliminary numerical simulations. Newfoundland: Institute for Ocean Technology (IOT) Report No, TR-2010-24, 2010.

[21] J. Wang, A. Derradji-Aouat, Numerical assessment for stationary structure (Kulluk) in moving broken ice, in: Proceedings of the International Conference on Port and Ocean Engineering Under Arctic Conditions, 2011.
[22] A. Tsarau, R. Lubbad, S. Løset, A numerical model for simulation of the hydrodynamic interactions between a marine floater and fragmented sea ice, Cold Regions Science and Technology. 103 (2014) 1–14.
[23] A. Tsarau, S. Løset, Modelling the hydrodynamic effects associated with station-keeping in broken ice, Cold Regions Science and Technology. 118 (2015) 76–90.
[24] L.G. Bennetts, T.D. Williams, Water wave transmission by an array of floating discs, in: Proceedings of the Royal Society of London A: Mathematical, Physical and Engineering Sciences, The Royal Society, 2015: p. 20140698.
[25] L.J. Yiew, L.G. Bennetts, M.H. Meylan, B.J. French, G.A. Thomas, Hydrodynamic responses of a thin floating disk to regular waves, Ocean Modelling. 97 (2016) 52–64.
[26] F. Nelli, L.G. Bennetts, D.M. Skene, J.P. Monty, J.H. Lee, M.H. Meylan, A. Toffoli, Reflection and transmission of regular water waves by a thin, floating plate, Wave Motion. 70 (2017) 209–221.
[27] D.M. Skene, L.G. Bennetts, M.H. Meylan, A. Toffoli, Modelling water wave overwash of a thin floating plate, Journal of Fluid Mechanics. 777 (2015).
[28] H. Jasak, CFD Analysis in Subsea and Marine Technology, IOP Conf. Ser.: Mater. Sci. Eng. 276 (2017) 012009. https://doi.org/10.1088/1757-899X/276/1/012009.
[29] W. Bai, T. Zhang, D.J. McGovern, Response of small sea ice floes in regular waves: A comparison of numerical and experimental results, Ocean Engineering. 129 (2017) 495–506.
[30] L. Huang, G. Thomas, Simulation of Wave Interaction With a Circular Ice Floe, Journal of Offshore Mechanics and Arctic Engineering. 141 (2019) 041302.
[31] L. Huang, K. Ren, M. Li, Ž. Tuković, P. Cardiff, G. Thomas, Fluid-structure interaction of a large ice sheet in waves, Ocean Engineering. 182 (2019) 102–111.
[32] J. Wackers, B. Koren, H.C. Raven, A. Van der Ploeg, A.R. Starke, G.B. Deng, P. Queutey, M. Visonneau, T. Hino, K. Ohashi, Free-surface viscous flow solution methods for ship hydrodynamics, Archives of Computational Methods in Engineering. 18 (2011) 1–41.
[33] L. Huang, M. Li, T. Romu, A. Dolatshah, G. Thomas, Simulation of a ship operating in an open-water ice channel, Ships and Offshore Structures. 0 (2020) 1–10. https://doi.org/10.1080/17445302.2020.1729595.
[34] C.F. Jan\s sen, D. Mierke, T. Rung, On the development of an efficient numerical ice tank for the simulation of fluid-ship-rigid-ice interactions on graphics processing units, Computers & Fluids. 155 (2017) 22–32.
[35] S. Mintu, D. Molyneux, Simulation of Ice-Structure Interactions Using a Coupled SPH-DEM Method, in: OTC Arctic Technology Conference, Offshore Technology Conference, 2018.
[36] S. Mintu, Evaluation of Ice Management Performance Using SPH-DEM Approac, in: St. John's, Canada, 2018.
[37] L.A. Roach, M.M. Smith, S.M. Dean, Quantifying growth of pancake sea ice floes using images from drifting buoys, Journal of Geophysical Research: Oceans. 123 (2018) 2851–2866.
[38] S. Sun, H.H. Shen, Simulation of pancake ice load on a circular cylinder in a wave and current field, Cold Regions Science and Technology. 78 (2012) 31–39.
[39] L. Huang, M. Li, B. Igrec, P. Cardiff, D. Stagonas, G. Thomas, Simulation of a ship advancing in floating ice floes, in: Port and Ocean Engineering under Arctic Conditions (POAC), 2019.
[40] W.J. Kim, S.H. Van, D.H. Kim, Measurement of flows around modern commercial ship models, Experiments in Fluids. 31 (2001) 567–578.
[41] ITTC, Guidelines: Practical Guidelines for Ship CFD Applications, ITTC Report. (2014).
[42] F. Menter, Zonal two equation kw turbulence models for aerodynamic flows, in: 23rd Fluid Dynamics, Plasmadynamics, and Lasers Conference, 1993: p. 2906.
[43] Z. Zhang, H. Liu, S. Zhu, F. Zhao, Application of CFD in ship engineering design practice and ship hydrodynamics, Journal of Hydrodynamics. 18 (2006) 308–315.
[44] C.W. Hirt, B.D. Nichols, Volume of fluid (VOF) method for the dynamics of free boundaries, Journal of Computational Physics. 39 (1981) 201–225.

[45] H.K. Versteeg, W. Malalasekera, An introduction to computational fluid dynamics: the finite volume method, Pearson Education, 2007.
[46] O. Baran, Discrete element method in STAR CCM+, in: STAR Japanese Conference, 2012.
[47] A. Polojärvi, J. Tuhkuri, O. Korkalo, Comparison and analysis of experimental and virtual laboratory scale punch through tests, Cold Regions Science and Technology. 81 (2012) 11–25.
[48] P. Mucha, Fully-Coupled CFD-DEM for Simulations of Ships Advancing Through Brash Ice, in: SNAME Maritime Convention, The Society of Naval Architects and Marine Engineers, 2019.
[49] W. Luo, D. Jiang, T. Wu, C. Guo, C. Wang, R. Deng, S. Dai, Numerical simulation of an ice-strengthened bulk carrier in brash ice channel, Ocean Engineering. 196 (2020) 106830.
[50] P.A. Cundall, O.D. Strack, A discrete numerical model for granular assemblies, Geotechnique. 29 (1979) 47–65.
[51] G.W. Timco, W.F. Weeks, A review of the engineering properties of sea ice, Cold Regions Science and Technology. 60 (2010) 107–129.
[52] J.H. Holland, Adaptation in natural and artificial systems: an introductory analysis with applications to biology, control, and artificial intelligence, MIT press, 1992.
[53] P. Wadhams, A mechanism for the formation of ice edge bands, Journal of Geophysical Research: Oceans. 88 (1983) 2813–2818.
[54] F. Parmiggiani, M. Moctezuma-Flores, P. Wadhams, G. Aulicino, Image processing for pancake ice detection and size distribution computation, International Journal of Remote Sensing. (2018) 1–16.
[55] H. Gong, A. Polojärvi, J. Tuhkuri, Discrete element simulation of the resistance of a ship in unconsolidated ridges, Cold Regions Science and Technology. (2019) 102855.
[56] S.P. Bateman, M.D. Orzech, J. Calantoni, Simulating the mechanics of sea ice using the discrete element method, Mechanics Research Communications. 99 (2019) 73–78.
[57] M. van den Berg, R. Lubbad, S. Løset, The effect of ice floe shape on the load experienced by vertical-sided structures interacting with a broken ice field, Marine Structures. 65 (2019) 229–248.
[58] J. Paavilainen, J. Tuhkuri, Pressure distributions and force chains during simulated ice rubbling against sloped structures, Cold Regions Science and Technology. 85 (2013) 157–174.
[59] A. Polojärvi, J. Tuhkuri, A. Pustogvar, DEM simulations of direct shear box experiments of ice rubble: Force chains and peak loads, Cold Regions Science and Technology. 116 (2015) 12–23.